

Design and Screening of Metal–Organic Frameworks for Ethane/Ethylene Separation

Seunghee Han and Jihan Kim*

Cite This: *ACS Omega* 2023, 8, 4278–4284

Read Online

ACCESS |



Metrics & More

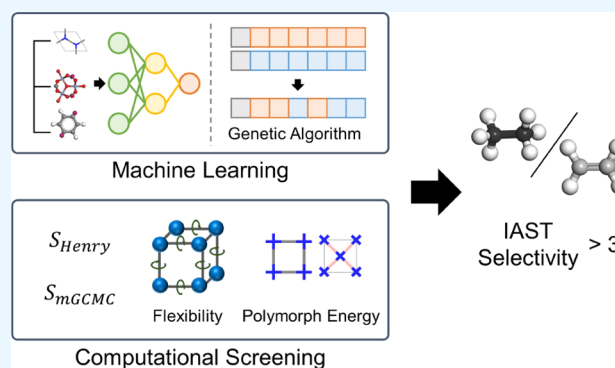


Article Recommendations



Supporting Information

ABSTRACT: Separation of ethane and ethylene is considered to be industrially important for various chemical processes, but their similarities make the process expensive. In this study, we integrated computational screening with machine learning to find optimal metal–organic frameworks (MOFs) with high ethane/ethylene selectivity. Using our algorithm, a hypothetical MOF structure with an ideal adsorption solution theory selectivity of 3.6 at 298 K and 1 bar was discovered. Furthermore, structural analysis was implemented, and the full adsorption isotherm of some of the top structures was obtained.



INTRODUCTION

Separation of ethane and ethylene is industrially important as power plants produce large amounts of chemicals like olefins that include ethane and ethylene.^{1,2} However, the separation of two molecules is extremely difficult due to their similar properties. As such, purification of ethane and ethylene is a very energy-intensive process, which to this date, relies on conventional repeated cryogenic distillation.^{3–5} Therefore, demand for more efficient and less-energy separation method is increasing.

To remedy this situation, adsorption through porous materials has been suggested as an alternative method for separation. In particular, metal–organic frameworks (MOFs) are a class of porous materials consisting of metal clusters coordinated to organic linkers, which combines the characteristics of both organic and inorganic materials. MOFs are used for various functionalities, such as chemical species separation, gas storage, catalyst, drug delivery, and chemical sensors.^{6–9}

So far, both ethane-selective MOFs and ethylene-selective MOFs have been reported.¹⁰ MOFs that selectively adsorb ethylene usually involve distinct characteristics like open metal sites or polar elements.^{11–13} However, the ethylene-selective structures can be vulnerable to water given that these strong binding metal sites attract water molecules.¹⁴ In addition, strategies that adsorb ethylene needs further purification because the remaining ethane can contaminate the ethylene product during the desorption stages, and ethane-selective MOFs can also be helpful in this process.^{15–17} From this point of view, resorting to selective adsorption for ethane might be an important strategy. Nevertheless, since ethane has relatively low polarity, the reported selectivity of ethane-selective MOFs

is low.¹⁸ As far as we know, the highest reported ethane-selective MOF is 4.3 [Fe₂(dobdc) by Li et al.,¹⁹ whereas most MOFs range between 1 to 3 for ethane/ethylene selectivity.

To expedite the search for high-performance ethane-selective MOFs, various screening studies have been conducted using database of MOFs, such as the CoRe MOF database²⁰ and the h-MOF database.²¹ Tang and Jiang identified 16 MOFs with C₂H₆/C₂H₄ > 2.16 and ethane uptake > 0.54 mol/kg in the CoRe MOF database,²² and Halder and Singh discovered four MOFs with C₂H₆/C₂H₄ > 2.7 in h-MOF database.²³ Unfortunately, these studies are limited by the structures populating the existing database, and as such, it is difficult to go beyond what is reported within these relatively small number of materials. To remedy this issue, Lee et al. adopted an inverse-design approach and constructed a top-down generator called the PORMAKE, to integrate deep learning and genetic algorithm and to explore trillions of MOFs.²⁴ In this work, we used PORMAKE and its workflow to design MOFs with the user-desired high ethane/ethylene selectivity to expand the search space for high-performance ethane-selective MOFs.

Received: November 23, 2022

Accepted: January 5, 2023

Published: January 18, 2023



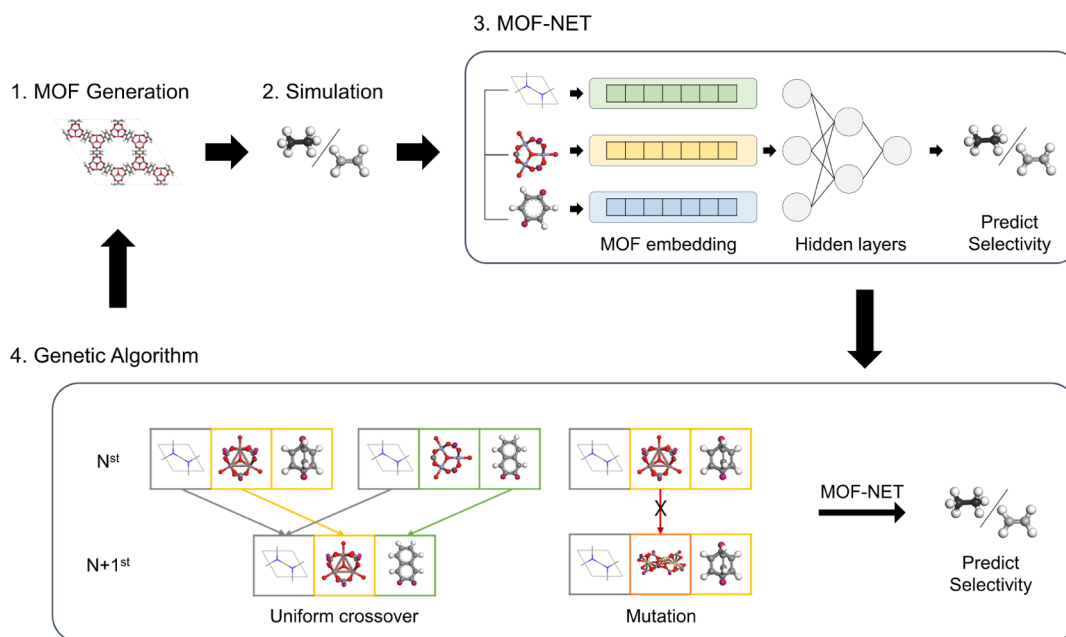


Figure 1. Schematics of the screening process with high selectivity. MOF-NET is trained from the simulation results, and a new candidate MOF set is predicted through a genetic algorithm.

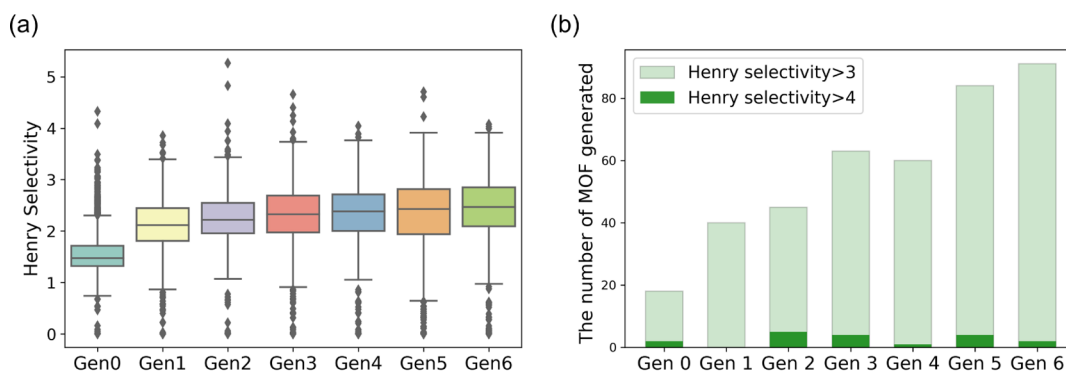


Figure 2. Distribution results of the structures for each generation. (a) Box plot for each generation's Henry selectivity. (b) Data distribution of the structures with high selectivity (empty: Henry selectivity > 3 and filled green: selectivity > 4).

RESULTS AND DISCUSSION

Screening of High Selectivity MOFs. Initially, 4984 hypothetical MOFs were constructed randomly using POR-MAKE. The Henry coefficient of ethane ($K_{\text{H}_2\text{C}_2\text{H}_6}$) and ethylene ($K_{\text{H}_2\text{C}_2\text{H}_4}$) was computed using RASPA²⁵ software to obtain the selectivity ($S = K_{\text{H}_2\text{C}_2\text{H}_6}/K_{\text{H}_2\text{C}_2\text{H}_4}$) for each of these MOFs. With these data, the model to predict the selectivity was trained using a regression deep learning model called the MOF-NET.²⁴ Finally, the optimal structures predicted to have high ethane selectivity were extracted using the genetic algorithm and generated by PORMAKE. The overall process is illustrated in Figure 1, and this procedure was repeated many times until performance saturation.

For each generation, about 500 to 1000 hypothetical structures were constructed, resulting in the improved mean performance for ethane/ethene selectivity (see Figure 2a) as well as discovery of high selective (i.e., $S > 3$) MOFs, as shown in Figure 2b (Supporting Information, S1). This process was repeated six times, and a total of 8676 MOFs were generated. At the end, the MOF with the highest selectivity was 5.26, and

its structural information is described in Supporting Information, S3 (Figure S4). Using our algorithm, 16 structures with $S > 4$ and 401 structures with $S > 3$ were discovered. The process of filtering these generated structures into the final candidates is shown in Figure 3.

From the reduced set of 401 structures, multicomponent grand-canonical Monte Carlo (m-GCMC) adsorption simulations were performed for more detailed analysis. In most of

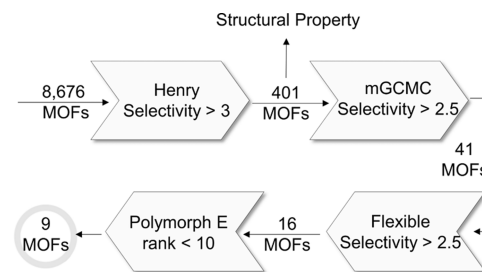


Figure 3. Detailed process of filtering the structures with appropriate criteria after generation of MOFs.

the experiments, the selectivity of ethane/ethylene is determined by the ideal adsorption solution theory (IAST) selectivity at an equimolar ratio (1:1) of 1 bar and 298 K. The values of the IAST selectivity computed from the simulations and the selectivity computed by multicomponent GCMC simulation were very similar, which can be shown in Figure S3. Therefore, ethane/ethylene selectivity was additionally computed with the multicomponent GCMC simulations. While some structures showed selectivity values similar to their Henry coefficient selectivity values, in most cases the selectivity decreased compared to that from the Henry coefficient calculations (Figure 4). As a result, 41 structures with the $S > 2.5$ remained after the multi-component GCMC simulations with the highest being MOFs with IAST selectivity of 5.30 and 4.07 (Figure S5).

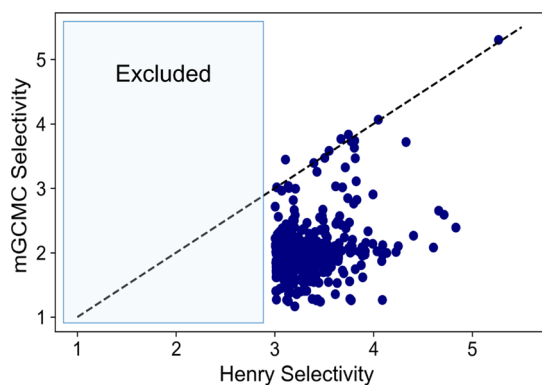


Figure 4. Relationship between the selectivity by Henry coefficients and the selectivity by multicomponent GCMC (each point represents a different MOF).

Next, the geometrical properties [i.e., void fraction (VF) and pore limiting diameter (PLD)] of the 401 structures were obtained using Zeo++ software.²⁶ The relationship between selectivity, VF, and PLD is illustrated in Figure 5. The data

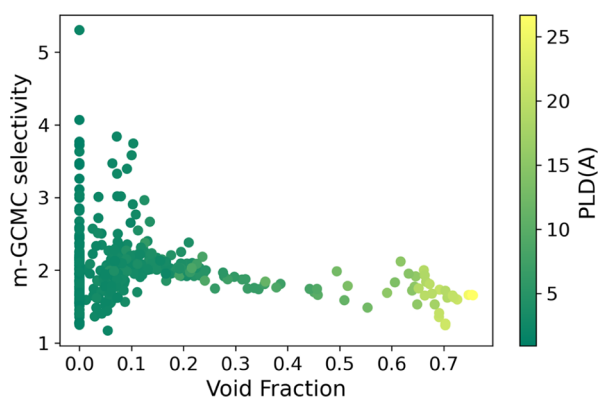


Figure 5. 401 MOF data points that illustrate the relationship between selectivity and VF/PLDs.

here show a similar pattern with previous papers that focused on the roles of VF and PLD in ethane/ethylene selectivity for MOFs.²³ The general pattern here implies that there is a trade-off between ethane adsorption (due to the low VF) and ethane selectivity.

Refined Analysis on Top Structures. In all of the previous results, simulations were conducted under the rigid

MOF assumption. However, given that some of these MOFs can showcase flexibility, we decided to consider flexibility on a selective set of the top 41 structures with $S > 2.5$. To account for flexibility, molecular dynamics (MD) simulations were conducted using LAMMPS software²⁷ on these top 41 structures. The *NVT* simulations were conducted for 1.2 ns (0.2 ns for equilibrium steps and 1 ns for production steps) at $T = 298$ K, and five snapshots were taken for every 200 ps (where the selectivity values were averaged from these snapshot configurations, see the Methods section for more detail). Removing structures with structural errors and LAMMPS interface issues, 30 structures remained for analysis. The overall results show that selectivity generally tends to decrease slightly (Figure 6). It was observed that 16 structures

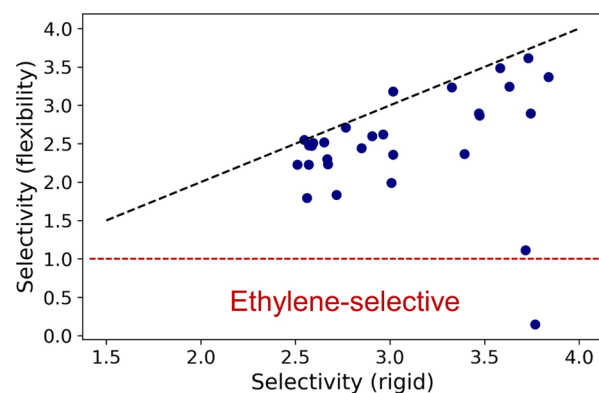


Figure 6. Comparison between m-GCMC selectivity values obtained from rigid and flexible simulations.

have $S > 2.5$ after incorporating flexibility while some structures even changed to being ethylene-selective ($S < 1$). The ethylene-selective structures have linkers which can affect the pores of the frameworks when rotating around the connection axis (Figure S6).

In this study, the hypothetical structures were generated based on topology, which allowed multiple polymorphs to be formed using the same MOF components. Therefore, to obtain synthesizable feasibilities for each of the polymorphs, the total energies were compared. In our analysis, structures with high energy among polymorphs (i.e., energy rank > 10) were excluded as they were deemed to be unsynthesizable. Using these criteria, a total of nine MOFs with high selectivity survived in the analysis. The final selectivity and ethane uptake for these nine MOFs are shown in Figure 7. Specific information about these structures can be found in Supporting Information, S3 (Table S3).

In the end, the two final structures with $S > 3$ are illustrated in Figure 8a,b. The MOF with the highest selectivity of 3.6 and the lowest energy among the polymorphs was identified to be comprising Co node building block (NBB) and barrelene edge building block (EBB) (Figure 8a). The metal node is the same one used in MUF-15¹⁴ (with different linker), which has reported an experimental selectivity of 2.0. The MOF with the second highest selectivity ($S = 3.4$) was composed of Cu NBB and cyclohexane EBB (Figure 8b). These two MOFs have the small and rotational invariant EBB compared to other linkers in common, and as such flexibility made little difference in the shape of the pores, which kept the selectivity high in the flexible simulations.

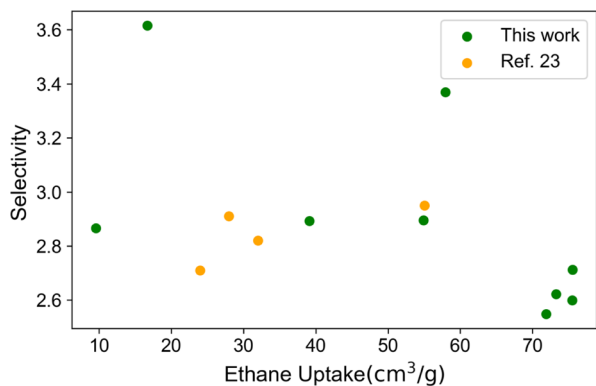


Figure 7. Final selectivity and ethane uptake of final nine MOFs (each point indicates each MOFs).

The mixture adsorption isotherm curves computed from the GCMC simulations of the two structures are shown in Figure 8c,d. Ethane and ethylene adsorption in both structures were saturated at very small pressures; therefore, the selectivity was maintained when the pressure approaches to 1 bar. This correlates with the similarity of Henry selectivity and m-GCMC selectivity of these structures (see Supporting Information, S4).

The structure of the former adsorbs about 13.2 cm³/g of ethane for equimolar C₂H₆/C₂H₄ mixture at 298 K and 1 bar. However, the structure of the latter adsorbs about 46.5 cm³/g under the same condition. Therefore, it can be seen the latter (pcu + N489 + E151) has slightly smaller selectivity, but it can be seen that ethane can be adsorbed better.

CONCLUSIONS

In this study, MOFs with high selectivity were generated using an integrated machine learning (ML) and genetic algorithm model. We computed selectivity with the Henry coefficient for ML and screening and then recalculated the selectivity through m-GCMC simulation for both the computational cost and the accuracy. We generated 41 structures with m-GCMC selectivity >2.5, then reduced the optimal candidate structures further by applying several criteria, and identified two structures with $S > 3$. In particular, it is meaningful these selectivity values took MOF flexibility into account, which in general reduces the selectivity values compared to the rigid MOF case. The final two structures possess rotational invariant linkers and are saturated at very low pressure. Through structural analysis, it can be concluded that a trade-off may occur between selectivity and adsorption amount in MOFs, which makes it difficult to obtain high selectivity and large amount of adsorption at the same time. Finally, we have demonstrated that our algorithm is helpful and efficient for

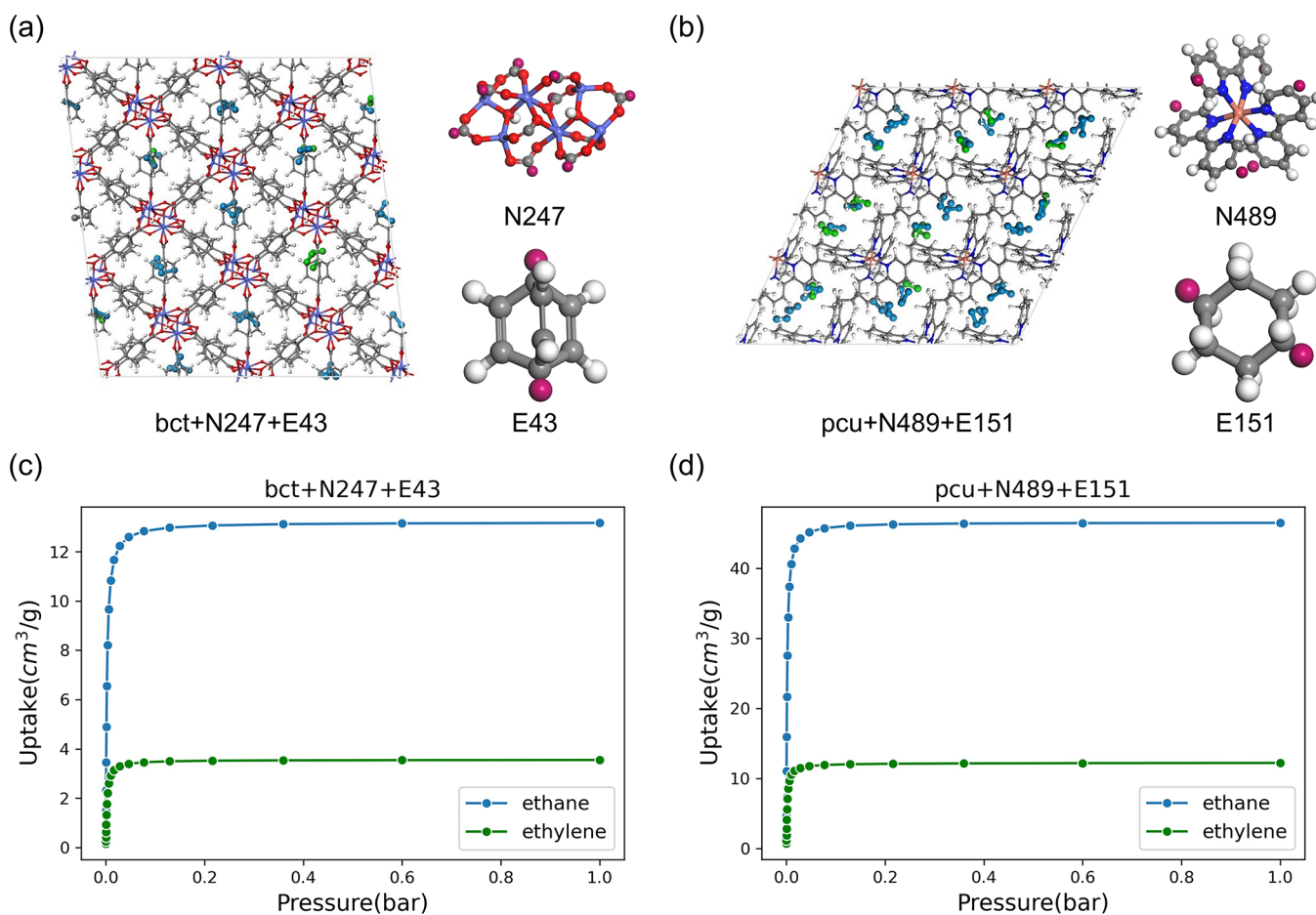


Figure 8. View and IAST adsorption of the final two structures [for equimolar ratio (1:1) at 298 K]. (a) View of bct + N247 + E43, (b) view of pcu + N489 + E151 (cobalt blue: Co, red: O, gray: C, white: H, orange: Cu, blue: N, purple: connection point, green: ethane, and yellow: ethylene), (c) IAST adsorption of bct + N247 + E43, and (d) IAST adsorption of pcu + N489 + E151.

designing and generating MOFs with user-desired properties and can serve as meaningful workflow for other energy and environmental related applications.

METHODS

Generation of Random MOFs. Hypothetical MOFs were generated by PORMAKE,²⁴ which is top-down method to construct MOFs with NBBs and EBBs based on topology. The details of each component and generating MOFs were explained in a study by Lee et al. In this study, 41 topologies, 756 NBB, and 158 EBB were used to construct MOFs. The structures were discarded if the number of atoms per cell exceeds 2500. The structures containing metals in both NBBs and EBBs were excluded in consideration of the stability. In addition, the structures not containing metals in both NBBs and EBBs, which are called covalent–organic frameworks (COFs), were excluded. The generated MOFs were optimized by the Forcite Module of Material Studio²⁸ before molecular simulation.

Machine Learning. The model of ML is based on MOF-NET,²⁴ the artificial neural network model using the embedding technique similar to Word2Vec.²⁹ It can map topologies and building blocks (BBs) to a pre-determined length vector. Through this technique, these vectors are also trained in the ML process, and the interaction or importance of topology and BBs can be turned out. In the MOF-NET, the data set was composed of target feature (selectivity) and the names of MOFs (topology + NBBs + EBBs). Using MOF-NET, the model to predict selectivity by the Henry coefficient was constructed and used for fitness function of genetic algorithm.

The genetic algorithm was taken from the multispecies genetic algorithm with fitness approximation (MSGFA-FA) of Lee et al.²⁴ This algorithm calculates the fitness values (selectivity predicted from the MOF-NET) of chromosomes composed of the names of NBBs and EBBs for each topology. The chromosomes of MOFs with the high fitness value for each topology were adopted. Then, the selectivity of adopted MOFs was computed through Henry's constant through molecular simulation again, and this process was repeated.

Selectivity Approximation. The selectivity data were required to train the ML model, and it can be attained directly through molecular simulation. In this work, selectivity was approximated in two ways: Henry coefficient calculation and m-GCMC calculation.

The selectivity calculated by Henry's constant was used for ML and genetic algorithms. This approximation is used to reduce the computational cost. The Henry selectivity was calculated for 17 experimental data, and the tendency was consistent with the experimental selectivity values to some extent (Figure S2). The discrepancy between the experimental value and the simulation may be due to the error that comes from approximating the selectivity with the Henry coefficient. The equation of calculating the selectivity of ethane/ethylene by the Henry coefficient is shown in the following equation.

The ethane/ethylene selectivity

$$= \frac{\text{the Henry coefficient of ethane } (K_{H,C_2H_6})}{\text{the Henry coefficient of ethylene } (K_{H,C_2H_4})}$$

The Henry coefficient of each MOF was calculated using the Widom insertion method³⁰ via RASPA. The atoms of MOFs

were represented by Lennard-Jones (LJ) potential with the parameters of the universal force field.³¹ The ethane and ethylene molecules were assumed the united-atom model with the parameters of the TraPPE force field.³² The justification for using these parameters was discussed already by Tang and Jiang.²² The parameters applied between all the atoms were calculated using the Lorentz–Berthelot mixing rule. The cutoff distance was set to 12.8 Å for the LJ interactions. Each simulation was performed with 50,000 cycles for the error less than 5%. The temperature was considered at 298 K.

m-GCMC was conducted for 401 structures with the Henry selectivity $S > 3$. In the experiment, the selectivity of ethane and ethylene was usually assumed through IAST at the condition of equimolar mixture, 298 K and 1 bar. The IAST selectivity is calculated using the following equation.³³

$$S_{C_2H_6/C_2H_4} = \frac{x_{C_2H_6}/x_{C_2H_4}}{y_{C_2H_6}/y_{C_2H_4}}$$

In the equation, x_i is the mole fraction of the adsorbed phase, and y_i is the mole fraction of the bulk phase. We assumed the equimolar mixtures, so $y_{C_2H_6}/y_{C_2H_4}$ was set to be 1. The relative amounts adsorbed ($x_{C_2H_6}/x_{C_2H_4}$) can be calculated through multi-component GCMC in RASPA simulation. The parameters between all of the atoms are identical to above simulation. The Monte Carlo adsorption simulation component information consists of translation probability, rotation probability, identity change probability, and swap probability. These probabilities were set to 0.15, 0.15, 0.1, and 0.6 used from the previous studied paper.²³ The mole fraction of ethane is 0.5. The simulation was performed at 298 K and 1 bar.

The program IAST++ was used for IAST calculation and IAST adsorption isotherm at various pressures.³⁴ GCMC simulation was performed on each ethane and ethylene at 10, 100, 1000, 10,000, 50,000, and 100,000 Pa. Each adsorption isotherm graph was drawn using IAST++ from above results. The isotherm approximation model was selected with the highest R^2 value of the fitting results. Then, IAST calculation was performed using the isotherm graph.

Analysis of the Structures with High Selectivity. The structures of MOFs considering flexibility can be figured out by the method of Gee and Sholl.^{2,35} This method entails the NVT simulation to incorporate the flexibility of the structures. The NVT simulation was conducted for 1.2 ns (0.2 ns for equilibrium steps and 1 ns for production steps) by LAMMPS,²⁷ and five snapshots were captured for every 200 ps. Then, m-GCMC simulation to get the selectivity was implemented for each snapshot, and the averaged values were calculated.

The polymorph of each MOF was generated for evaluating the structural stability and synthesizability of the MOF. Here, the polymorph refers to the structure which has the same NBBs and EBBs but a different topology (e.g., MIL-88B and MIL-101) from each MOF. The different topologies of the same connection point with the MOF were discovered, and the polymorphs with these topologies were generated. The total energy was calculated during the optimization of the polymorph through the Forcite Module of Material Studio.²⁸ Then, the energy was divided by the number of the metal atoms and compared to each other.

The VF and PLD were obtained by Zeo++ software.²⁶ The pore size was analyzed for the structures with the selectivity by the Henry coefficient above 3.

■ ASSOCIATED CONTENT

SI Supporting Information

The Supporting Information is available free of charge at <https://pubs.acs.org/doi/10.1021/acsomega.2c07517>.

Description of the results for ML and genetic algorithm; justification for the calculation of the selectivity; information of the structures with high selectivity; and results of IAST calculation (PDF)

■ AUTHOR INFORMATION

Corresponding Author

Jihan Kim – Department of Chemical and Biomolecular Engineering, Korea Advanced Institute of Science and Technology, Daejeon 34141, Republic of Korea;
orcid.org/0000-0002-3844-8789; Email: jihankim@kaist.ac.kr

Author

Seunghye Han – Department of Chemical and Biomolecular Engineering, Korea Advanced Institute of Science and Technology, Daejeon 34141, Republic of Korea;
orcid.org/0000-0001-8696-6823

Complete contact information is available at:
<https://pubs.acs.org/doi/10.1021/acsomega.2c07517>

Author Contributions

S.H. conceived the project and conducted molecular simulations and ML. J.K. directed the project. All authors contributed to discussing the project and writing the paper.

Notes

The authors declare no competing financial interest.

■ ACKNOWLEDGMENTS

This work was supported by the National Research Foundation of Korea (NRF) under project number 2021R1A2C200358312.

■ REFERENCES

- (1) Ren, T.; Patel, M.; Blok, K. Olefins from conventional and heavy feedstocks: Energy use in steam cracking and alternative processes. *Energy* **2006**, *31*, 425–451.
- (2) Agrawal, M.; Sholl, D. S. Effects of Intrinsic Flexibility on Adsorption Properties of Metal-Organic Frameworks at Dilute and Nondilute Loadings. *ACS Appl. Mater. Interfaces* **2019**, *11*, 31060–31068.
- (3) Sholl, D. S.; Lively, R. P. Seven chemical separations to change the world. *Nature* **2016**, *532*, 435–437.
- (4) Colón, Y. J.; Gómez-Gualdrón, D. A.; Snurr, R. Q. Topologically Guided, Automated Construction of Metal–Organic Frameworks and Their Evaluation for Energy-Related Applications. *Cryst. Growth Des.* **2017**, *17*, 5801–5810.
- (5) Sadrameli, S. M. Thermal/catalytic cracking of liquid hydrocarbons for the production of olefins: A state-of-the-art review II: Catalytic cracking review. *Fuel* **2016**, *173*, 285–297.
- (6) Li, H.; Wang, K.; Sun, Y.; Lollar, C. T.; Li, J.; Zhou, H.-C. Recent advances in gas storage and separation using metal-organic frameworks. *Mater. Today* **2018**, *21*, 108–121.
- (7) Lee, J.; Farha, O. K.; Roberts, J.; Scheidt, K. A.; Nguyen, S. T.; Hupp, J. T. Metal-organic framework materials as catalysts. *Chem. Soc. Rev.* **2009**, *38*, 1450–1459.
- (8) Lawson, H. D.; Walton, S. P.; Chan, C. Metal-Organic Frameworks for Drug Delivery: A Design Perspective. *ACS Appl. Mater. Interfaces* **2021**, *13*, 7004–7020.
- (9) Yi, F.-Y.; Chen, D.; Wu, M.-K.; Han, L.; Jiang, H.-L. Chemical Sensors Based on Metal-Organic Frameworks. *ChemPlusChem* **2016**, *81*, 675–690.
- (10) Wang, H.; Luo, D.; Velasco, E.; Yu, L.; Li, J. Separation of alkane and alkene mixtures by metal-organic frameworks. *J. Mater. Chem. A* **2021**, *9*, 20874–20896.
- (11) Geier, S. J.; Mason, J. A.; Bloch, E. D.; Queen, W. L.; Hudson, M. R.; Brown, C. M.; Long, J. R. Selective adsorption of ethylene over ethane and propylene over propane in the metal-organic frameworks M2(dobdc) (M = Mg, Mn, Fe, Co, Ni, Zn). *Chem. Sci.* **2013**, *4*, 2054–2061.
- (12) Bachman, J. E.; Kapelewski, M. T.; Reed, D. A.; Gonzalez, M. I.; Long, J. R. M2(m-dobdc) (M = Mn, Fe, Co, Ni) Metal-Organic Frameworks as Highly Selective, High-Capacity Adsorbents for Olefin/Paraffin Separations. *J. Am. Chem. Soc.* **2017**, *139*, 15363–15370.
- (13) Zhang, L.; Li, L.; Hu, E.; Yang, L.; Shao, K.; Yao, L.; Jiang, K.; Cui, Y.; Yang, Y.; Li, B.; Chen, B.; Qian, G. Boosting Ethylene/Ethane Separation within Copper(I)-Chelated Metal-Organic Frameworks through Tailor-Made Aperture and Specific π -Complexation. *Adv. Sci.* **2020**, *7*, 1901918.
- (14) Qazvini, O. T.; Babarao, R.; Shi, Z.-L.; Zhang, Y.-B.; Telfer, S. G. A Robust Ethane-Trapping Metal-Organic Framework with a High Capacity for Ethylene Purification. *J. Am. Chem. Soc.* **2019**, *141*, 5014–5020.
- (15) Silva, F. A. D.; Rodrigues, A. E. Propylene/propane separation by vacuum swing adsorption using 13X zeolite. *AIChE J.* **2001**, *47*, 341–357.
- (16) Bloch, E. D.; Queen, W. L.; Krishna, R.; Zadrozny, J. M.; Brown, C. M.; Long, J. R. Hydrocarbon Separations in a Metal-Organic Framework with Open Iron(II) Coordination Sites. *Science* **2012**, *335*, 1606–1610.
- (17) Wang, Y.; Hu, Z.; Cheng, Y.; Zhao, D. Silver-Decorated Hafnium Metal-Organic Framework for Ethylene/Ethane Separation. *Ind. Eng. Chem. Res.* **2017**, *56*, 4508–4516.
- (18) Liao, P.-Q.; Zhang, W.-X.; Zhang, J.-P.; Chen, X.-M. Efficient purification of ethene by an ethane-trapping metal-organic framework. *Nat. Commun.* **2015**, *6*, 8697.
- (19) Li, L.; Lin, R.-B.; Krishna, R.; Li, H.; Xiang, S.; Wu, H.; Li, J.; Zhou, W.; Chen, B. Ethane/ethylene separation in a metal-organic framework with iron-peroxo sites. *Science* **2018**, *362*, 443–446.
- (20) Chung, Y. G.; Haldoupis, E.; Bucior, B. J.; Haranczyk, M.; Lee, S.; Zhang, H.; Vogiatzis, K. D.; Milisavljevic, M.; Ling, S.; Camp, J. S.; Slater, B.; Siepmann, J. I.; Sholl, D. S.; Snurr, R. Q. Advances, Updates, and Analytics for the Computation-Ready, Experimental Metal-Organic Framework Database: CoRE MOF 2019. *J. Chem. Eng. Data* **2019**, *64*, 5985–5998.
- (21) Wilmer, C. E.; Leaf, M.; Lee, C. Y.; Farha, O. K.; Hauser, B. G.; Hupp, J. T.; Snurr, R. Q. Large-scale screening of hypothetical metal-organic frameworks. *Nat. Chem.* **2011**, *4*, 83–89.
- (22) Tang, H.; Jiang, J. In silico screening and design strategies of ethane-selective metal-organic frameworks for ethane/ethylene separation. *AIChE J.* **2021**, *67*, No. e17025.
- (23) Halder, P.; Singh, J. K. High-Throughput Screening of Metal-Organic Frameworks for Ethane-Ethylene Separation Using the Machine Learning Technique. *Energy Fuels* **2020**, *34*, 14591–14597.
- (24) Lee, S.; Kim, B.; Cho, H.; Lee, H.; Lee, S. Y.; Cho, E. S.; Kim, J. Computational Screening of Trillions of Metal-Organic Frameworks for High-Performance Methane Storage. *ACS Appl. Mater. Interfaces* **2021**, *13*, 23647–23654.
- (25) Dubbeldam, D.; Calero, S.; Ellis, D. E.; Snurr, R. Q. RASPA: molecular simulation software for adsorption and diffusion in flexible nanoporous materials. *Mol. Simul.* **2016**, *42*, 81–101.
- (26) Willems, T. F.; Rycroft, C. H.; Kazi, M.; Meza, J. C.; Haranczyk, M. Algorithms and tools for high-throughput geometry-

based analysis of crystalline porous materials. *Microporous Mesoporous Mater.* **2012**, *149*, 134–141.

(27) Plimpton, S. Fast Parallel Algorithms for Short-Range Molecular Dynamics. *J. Comput. Phys.* **1995**, *117*, 1–19.

(28) BIOVIA, Material Studio. *Dassault Systemes*, 2019.

(29) Mikolov, T.; Chen, K.; Corrado, G.; Dean, J. Efficient Estimation of Word Representations in Vector Space. **2013**, arXiv preprint arXiv:1301.3781.

(30) Dullens, R. P. A.; Aarts, D. G. A. L.; Kegel, W. K.; Lekkerkerker, H. N. W. The Widom insertion method and ordering in small hard-sphere systems. *Mol. Phys.* **2005**, *103*, 3195–3200.

(31) Rappe, A. K.; Casewit, C. J.; Colwell, K. S.; Goddard, W. A.; Skiff, W. M. UFF, a full periodic table force field for molecular mechanics and molecular dynamics simulations. *J. Am. Chem. Soc.* **1992**, *114*, 10024–10035.

(32) Martin, M. G.; Siepmann, J. I. Transferable Potentials for Phase Equilibria. 1. United-Atom Description of n-Alkanes. *J. Phys. Chem. B* **1998**, *102*, 2569–2577.

(33) Myers, A. L.; Prausnitz, J. M. Thermodynamics of mixed-gas adsorption. *AIChE J.* **1965**, *11*, 121–127.

(34) Lee, S.; Lee, J. H.; Kim, J. User-friendly graphical user interface software for ideal adsorbed solution theory calculations. *Korean J. Chem. Eng.* **2018**, *35*, 214–221.

(35) Gee, J. A.; Sholl, D. S. Effect of Framework Flexibility on C8 Aromatic Adsorption at High Loadings in Metal-Organic Frameworks. *J. Phys. Chem. C* **2016**, *120*, 370–376.